ORIGINAL SCIENTIFIC PAPER OPEN ACCESS

Using simulated data in computationally intelligent photoacoustics

Miroslava Jordović Pavlović[1], Miroslava Raspopović Milić[1*], Katarina Đorđević[2], Mioljub Nešić[2], Marica Popović[3]

[1] Metropolitan University, Faculty of Information Technology, Belgrade, Serbia

[2] Vinča Institute of Nuclear Sciences, Belgrade, Serbia

[3] Institute of Physics, Laboratory for Photoacoustic, Belgrade, Serbia

ARTICLE INFO

* **Correspondence:** miroslava.raspopovic@metropolitan.ac.rs

DOI: 10.5937/engtoday2300007J

UDC: 621(497.11) **ISSN:** 2812-9474

Article history: Received 28 April 2023; Revised 9 June 2023; Accepted 23 June 2023

ABSTRACT

A development of simulated data and discussion on potential use in processing photoacoustic measurement data, as well as in solving of an inverse problem are presented in the paper. Simulated experimental values are obtained based on theoretical-mathematical model of photoacoustic response, described in the paper. Credibility of the data is acquired due to the experimental measurements. Simulated data validity was proven with the satisfactory accuracy, precision, and reliability of the several machine learning models which were trained on the designed database and are applied in processing photoacoustic measurement data. Presented results show that if a huge dataset of high-quality data is generated, solving issues of inverse photoacoustic problem is successful, computing is cost effective, and process rate of machine learning models is suitable for real time work.

KEYWORDS

Simulated data, Theoretical-mathematical model, Artificial neural networks, Photoacoustics, microphone, Classification, Regression

1. INTRODUCTION

When some kind of pattern exists between input and output parameters of machine learning algorithm, and sufficient data is available for training of the algorithm, the pattern can be discovered or approximated. Eventually, newly discovered pattern will enable accurately calculating of output for inputs of interest outside the training dataset. If the training set quantity and quality are adequate, output for any future input could be estimated [1]. Hence, machine learning algorithms, and especially artificial neural networks (ANN), are widely accepted as tools for reliable and fast prediction in various domains. In the last few years, they are considered suitable for decision making in photoacoustics (PA), as one of photothermal (PT) methods, for solving issues that resisted standard procedures: the elimination of noise in image identification using photoacoustics [2], the improvement of atmosphere gases monitoring - contemporaneously laser beam spatial profile and polyatomic molecules relaxation time definition in gases in real time [3][4], the reconstruction of optical profile based on measured PT response [5], etc.

The material properties the most affect the recorded PA signal, but the measuring chain, particularly the microphone, also impacts the recorded signal, especially on its ends. This influence of the measured chain can significantly narrow the measurement range and reduce the accuracy of the solution to the inverse PA problem. Therefore, it is very important to recognize and describe the influence of the components of the measurement system. Neural networks are proving to be a very effective method for solving this problem.

Namely, physical properties resolution of the examined sample from its PA response is the goal of PA measurements. All PT methods are indirect measurement techniques, so is photoacoustics. Mathematically, it is an inverse problem. Generally, obtaining physical properties by model-dependent methods is done in two steps:

1. The first step is the **development of the direct model**. Mathematical model that adequately represent physical processes influenced by incident optical radiation and resulting in thermal response is created. Theoretical-mathematical modeling of temperature distribution within the sample, on sample surface, both front and back is done first. Secondly, modeling of PA response using obtained temperature variations is done…
2. The second step is **the development of the inverse procedure**. Sample physical properties determination due to gathered effects of designed mathematical model, measured PT response and common input parameters preset, such as characteristics of optical excitation - modulation frequency and intensity. Multiparameter fitting, complex numerical procedures and ANN are some of the inverse procedures. Concerning demanding examiner commitment and time consumption in a case of numerical procedures and fitting, they are not suitable regarding scientific and industrial application. These applications require real time procedures. ANNs are logical choice as a very effective ML algorithm.

The first requirement for the successful application of neural networks is quantity and quality of data, ANN is data hungry [6]. On the contrary, the facts with PA measurements are: firstly, numerous experimental collection that satisfy ANN request is hard to achieve, and on the other hand experimental data are risky due to influence of the measurement system, which is hidden in PA response [7]. The paper suggests another solution for obtaining a huge dataset: software which generates numerical experiments or simulated experimental data. A record in the obtained database consists of amplitude and phase instances of sampled simulated PA response. Credibility of simulated data is of great importance for precision of the new method. It is obtained thanks to expert knowledge.

In the past few years, the trend in machine learning is application of simulated data for training [8][9][10]. Concept of using simulated experimental data or numerical experiments generated by specially designed software based on developed theoretical-mathematical model for training ML models is new, as far as we know.

Firstly, the article explains a complete method of making a massive datasets of high-quality simulated data which will be used for training of ANN as the inverse solution of the inverse problem. Then, the review of latest achievements in PA material characterization research gained based on simulated data for aluminum are presented.

2. THEORETICAL-MATHEMATICAL MODEL OF PHOTOACOUSTIC RESPONSE

Photoacoustics is the first and most used photothermal method. All photothermal methods are based on the photothermal effect (the effect of generation of heat due to the absorption of the incident electromagnetic radiation from a wide spectrum of wavelengths). The heat generated in this way causes the disorder of the thermodynamic state of the sample (pressure, temperature, density) which propagates through the sample and the nearby environment, producing a number of detectable phenomena. Depending on the phenomenon being measured, there are different photothermal methods. In this article, we talk about gas-microphone photoacoustics where the oscillation of air pressure in PA cell, as a consequence of exposing the investigated sample to the modulated light beam, has been detected by a microphone[11].There are two types of photoacoustic cell, the first one is a so-called "reflection configuration", in which the source and the microphone are located on the same side of a sample, and the second one is the "transmission configuration", where a sample is placed between the source and the microphone. In our experimental setup, the minimum volume cell configuration is used. The minimum volume cell configuration is a kind of transmission cell configuration in which the sample is put directly on the top of the microphone, as presented in Figure 1, [12], so the microphone chamber becomes the PA cell, closed by the sample on one side and the microphone diaphragm on the other one. This kind of PA cell becomes the reason for disorders of the recorded signal on its endings [13], so if we want to utilize the whole measured frequency range, it is needed to know the behavior of the microphone.

On the other hand, in the case of reflective, or transparent and semitransparent materials, another layer is needed to increase the recorded signal level or to protect the microphone. Reflective materials have experimentally obtained signals low and in order to make the level of the recorded signal higher than the level of the noise (real–flicker noise, coherent signal deviation, and random noise), the absorption of the sample has to be large, and reflection has to be small, so we have to add another layer. In the case of transparent (or semitransparent) samples, the coefficient of transmission has to be increased because of the microphone protection.

In the case of transmission configuration, photoacoustic response is represented as sum of thermoconducting and thermoelastic component as two dominant signal components. Periodic heat flow from the sample to the surrounding gas (thermal-piston effect) influences thermoconducting component and thermoelastic banding of the sample (drum effect) influences thermoelastic component [14][15][16][17][18][19][20][21][22][25][26].

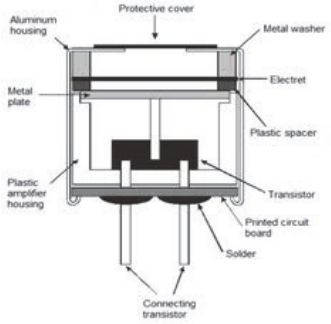

Figure 1: Photoacoustic experimental setup [12]

In our experiments two-layer structure is employed. The first layer is black coating, and the second layer is the investigated sample. Black coating is very thin, so it can be obtained as the first layer of the two-layer system on the one hand [23 - 26], but it also can be observed as a surface absorber of the incident radiation, and because of it as the surface heat source [14 - 20]. In the case of a large difference in the thickness of these two layers, it is better to use a theoretical mathematical model for a sample with surface absorption of incident radiation, because the influence of its thermal and elastic properties could not be observed in measuring range. Theoretical-mathematical expressions of PA response of both systems, used for obtaining the dataset, are given by following expressions:

$$\tilde{p}_{tot} = \tilde{p}_{th} + \tilde{p}_{ac} \tag{1}$$

$$\tilde{p}_{th} = \delta P = \frac{\gamma P_0}{l_g T_0} \frac{1}{\tilde{\sigma}_g} \tilde{\vartheta}(l_s) \tag{2}$$

$$\tilde{p}_{ac} = \frac{3\gamma P_0}{l_a} a_T \frac{R^2}{l_s^3} \int_0^{l_s} \left(x - \frac{l_s}{2} \right) \tilde{\vartheta}_s(x) dx \tag{3}$$

p_{tot} is total pressure recorded by photoacoustic, p_{th} is the thermoconducting component and p_{ac} is the thermoelastic component. P_0 represents cell presser, V_0 represents cell volume (V_0 represents the volume of the chamber cavity in the case of the minimum volume cell), γ is the heat capacity ratio, α_T is the thermal expansion coefficient, R_c is the radius of the chamber in front of the microphone diaphragm, while l_s is the sum of the thicknesses these two layers, and in the case of the very thin coating it can be observed as the thickness of the investigated sample. $\theta(x)$ act for temperature variations inside the samples and $\theta(l_s)$ act for surface temperature variation on the rare surface, and different expressions are used for these temperature variations for these two cases (one-layer or two-layer system) [14 - 20] .

Figure 2a) and 2b) describe appearance of simulated total pressure amplitude and phase characteristics, respectively.

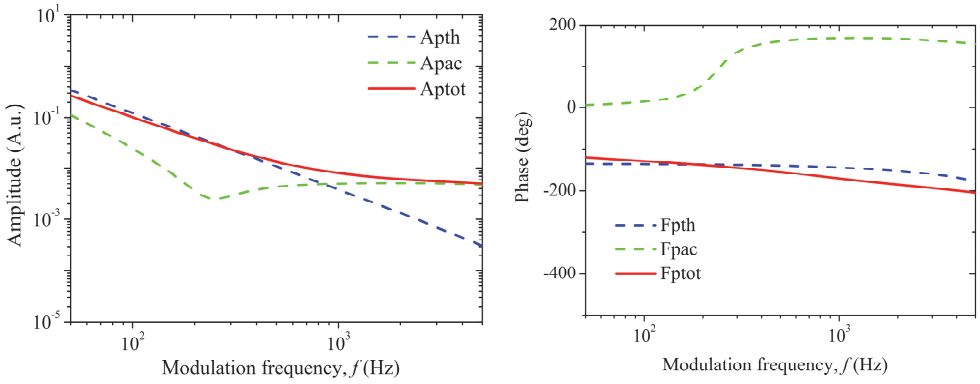

Figure 2: Simulated curves (amplitude and phase)) of the total photoacoustic signal, $p_{tot}(f)$, obtained by the designed software based on theoretical-mathematical model (solid line) and corresponding components $p_{th}(f)$ and $p_{ac}(f)$ (dotted lines).

Microphone acts as acoustic-electric converter and is the main part of the detector system in PA experiment of minimum volume cell [27]. Construction, applied geometry and membrane type influence microphone transfer function in both frequency and time domain. Concerning the literature [7] and experiments done by us, microphone behavior

could be described as filtering, thus at low frequencies (< 1 kHz) as electronic high-pass filters and at high frequencies (> 1 kHz) as acoustic low-pass filters.

The following mathematical expressions describe total transfer function of measurement chain influence, concerning the microphone as the component that has the greatest impact on signal distortion:

$$H_1^e(f) = \frac{1}{1 - j\frac{f_1}{f}} \tag{4}$$

$$H_2^e(f) = \frac{1}{1 - j\frac{f_2}{f}} \tag{5}$$

$$H^a(f) = \frac{f_3^2}{f_3^2 - f^2 + jff_3\xi_3} + \frac{f_4^2}{f_4^2 - f^2 + jff_4\xi_4} \tag{6}$$

$$H_{mic}(f) = H_2^e(f) H_{total}^a(f) \tag{7}$$

$$H_{total}(f) = H_1^e(f) H_{mic}(f) \tag{8}$$

Where, electronic characteristic of the influence of the other components like the sound card in the measurement chain is represented by $H_1^e(f)$ and characteristic frequency f_1. This frequency is considered constant due to experimental experience. Electronic and acoustic characteristics of microphone are presented as $H_2^e(f)$ and $H^a(f)$. f_2 corresponds to the characteristic frequency of the electronic high-pass filter and f_3 and f_4 to the characteristic frequencies of the acoustic low-pass filters of the microphone, ξ_3 and ξ_4 are reciprocal values of the quality factor, or, in other words, the double value of the damping factor. By multiplication these two components, microphone response is obtained. Microphone response amplitude and phase deviations are present and particularly persistent at the beginning and the end of frequency range. Different transfer functions are usual for different microphone types, but the difference happens even in the case of two microphones of the same type. There is no two identical microphones in practice. By multiplication of the total pressure and the total transfer function, theoretical-mathematical model for the total photoacoustic signal, recorded by the minimum volume cell photoacoustic experimental set up, is obtained:

$$S(f) = \sigma p_{total}(f) H_{total}(f) \tag{9}$$

Considering this equation and well known experiment preset, the database of simulated data or numerical PA experiments is obtained. Figure 3a) and 3b) depict amplitude and phase of distorted photoacoustic signal. According to experimental experience, the shape of all the curves is expected. Outliers do not exist.

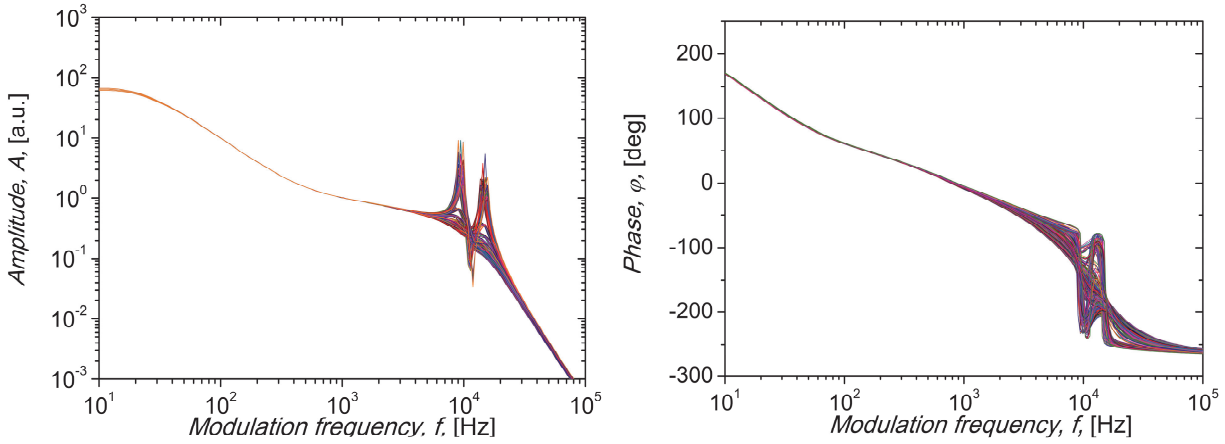

Figure 3: Distorted photoacoustic signals a) amplitude and b) phase. Curves with different microphone characteristics belong to dataset used for network training [28]

3. DATABASE DESCRIPTION

Software for database generation is designed using Matlab programming IDE. Preset of defined values corresponding to microphones: ECM30B, ECM60 and WM66, commonly used in PA experiments, is given in Table 1. One more mi-

crophone type will be observed here, and thus it is present in the dataset. So called ideal microphone (IM) is microphone of ideal behavior and is very important for distorted PA response correction. Response of PA ideal microphone is flat in a frequency range of interest that proves identical sensitivity and frequency independence. In the case of IM, PA response is not distorted, so corrections are needless and time is preserved.

The black dye-aluminum structure was investigated during the process of the examination. The thickness of aluminum plate used in experiment is 197 μm and its radius is 10 μm. The thickness of black ink dye layer that covers the plate is 2 μm. Table 1 presents predefined set of characteristics.

Table 1: Theoretical values for aluminum sample

	Dye	Aluminum
Thermal conductivity [$Wm^{-1}K^{-1}$]	70	210
Thermal diffusivity [m^2s^{-1}]	$2.5 \cdot 10^{-5}$	$8.6 \cdot 10^{-5}$
Thermal relaxation time [s]	10^{-4}	10^{-12}
Absorption coefficient [m^{-1}]	10^8	$145 \cdot 10^6$

Credibility of numerical experiments is obtained thanks to expert knowledge. Value ranges for each microphone parameter is specifically set due to its stability. Namely, considering repeatability in every measurement, different stability is appraised for individual microphone parameter. Microphone frequency f_2 is connected to its RC characteristics, so it is the most stable parameter. Only three values were set for creating simulated data. For microphone ECM30B, one central value $f_{20} = 25$ and two values less and bigger comparing to central value for 5% are set. Central value for ECM60, WM66 and IM are 14.25 Hz, 61.75 Hz, 0.475 Hz respectively and other corresponding values are 15Hz and 15.75 Hz, 65 Hz and 68.25 Hz, 0.5 Hz and 0.525 Hz. Characteristic frequencies f_3 and f_4 are less stable than f_2 because of their dependency on experimental conditions, so ten values in particular ranges are set for the description of their experimental behavior. The distance between these ten values is equal. 8930-9866 Hz is the range for f_3 and 13965-15432 is the range for f_4 in the case of ECM30B microphone. Same ranges for frequencies f_3 and f_4, 7980-8817Hz and 13015-14383 Hz, respectively are chosen for microphones ECM60 and WM66. 190000-209998 Hz is the range for IM frequency f_3 and 285000-314997 Hz is range for IM frequency f_4. The most unstable parameters are damping factors of the second order low-pass filter, ξ_3 and ξ_4, which are strongly dependent on experimental conditions. Based on the peak position at frequency axe of second order filter amplitude characteristics, value ranges for ξ_3 and ξ_4, were chosen. In limitary situation characterized with signal ultra damping, critical value of quality factor is Q=0.5. In the case of value changes from 1 to 100 for Q significant curve change happens, so $\xi_{3,4} \in [0.99, 0.015]$. For each type of microphone 15 values in selected range are randomly chosen.

Simulation of all possible experimental conditions was the aim of the assumed distribution. In our previous work [29], comparative analysis of concepts for solving the inverse problem in PA is presented. 65,000 paired curves, meaning both amplitude and phase data, are created, so the database has 65,000 records for every microphone type. Each record contains 200 instances of amplitude and 200 instances of phase sampled in the range 10Hz to 100kHz, in total 400. Presented distribution is set for electret microphones, frequently used in PA measurements but there is possibility of use microphones which membrane is made of different materials such as grapheme, mylar and nickel, that is way wide frequency domain is chosen.

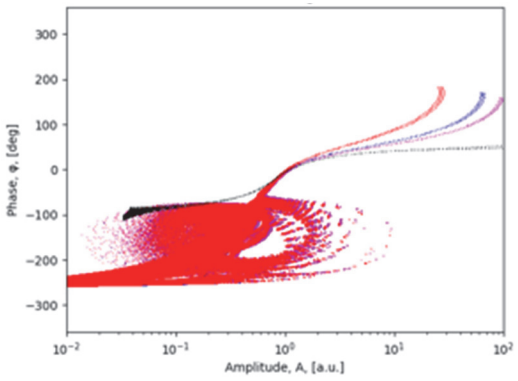

Figure 4: Scatter diagram of dataset [30]

Figure 4 provides data visualization in the form of scatter diagram. Two features describe each point on a scatter diagram, amplitude and phase. Data points belonging to different microphone types are differently colored. It can be concluded that classification to four classes is completely clear in upper-right part of the diagram which corresponds

to low frequency domain. Points are mixed in lower-left part of the diagram, curves (or classes) overlap, so it is questionable to which class point belongs. Training, validation and test set are obtained by dividing shuffled dataset in relation 90%, 5%, 5%, respectively. Randomly splitting provides generalization and reduces overfitting. Training set consists of 243 000 records, validation and test set have 13500 records each.

4. ESEARCH RESULTS AND DISCUSSION

This section is a review of research achievements based on simulated data for aluminum described earlier. The aim is to prove that simulated data created on the way suggested in the article are good solution and right research direction for training the models which provide answers for the inverse photoacoustic problem.

4.1. Application in photoacoustic measurement calibration

In the photoacoustic measurement setup (open-cell configuration photoacoustic spectroscopy) described in the previous section, the microphone with associated electronics and a phase-frequency (lock-in) amplifier plays a major role. Concerning distortions, the microphone has the greatest impact, and it should be further processed. A complete description of the microphone frequency response is necessary for the signal correction procedure. In order to obtain microphone transfer function, specific details that can be classified into several different classes and are related to the transfer function shape and the different levels of signal amplification and attenuation are needed. There are flat microphone response and generally shape microphone response. A flat response curve is an almost straight line, indicating that the measuring chain is approximately equally sensitive along the entire frequency range, so that the photoacoustic signal is transmitted without distortion. That is a case of the ideal microphone. Microphones frequently used in photoacoustic almost always have shape response curve. Its peaks and valleys indicate that the microphone is more sensitive at certain frequency bands compared to the others. The result is signal transmission with a certain degree of distortion, which must be detected.

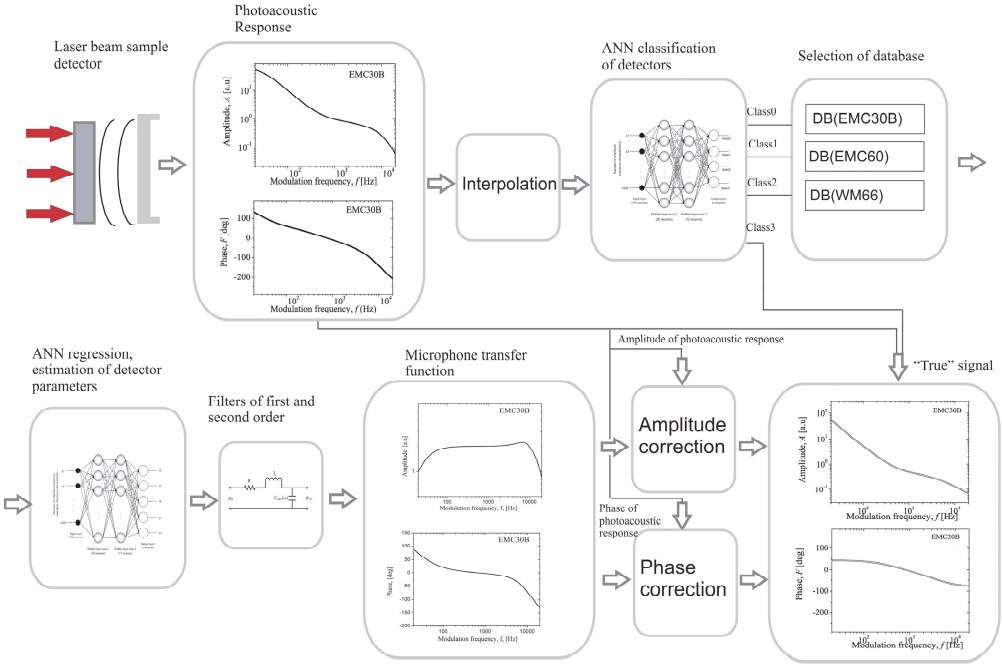

Figure 5: Photoacoustic measurement signal autocorrection method [28]

Figure 5 is block scheme of photoacoustics measurement signal autocorrection method which is result of our previous research. Microphone transfer function is detected from distorted PA experimental signal (sampled in a certain number of points) [28]. Main blocks of the scheme are regression and classification model trained on database of the mentioned numerical experiments. Method couples the results of regression and classification models. The form of transfer function corresponding to a specific microphone type is recognized by classification model. Then the regression model predicts numerical values of parameters (f_2, f_3, f_4, ζ_3, ζ_4) attributed to the shape of the transfer function [28]. Derived data are used by signal correction procedure, and as a result, transfer function of microphone used as a detector is subtracted from the real signal. The output of the method is undistorted experimental signal originated only from the used material sample. Obtained signal is used in the process of material characterization and finally physical parameters of the tested sample are accurately, precisely and reliably defined.

The classification model, Figure 6b) used in autocorrection method has the role of accelerating the process of processing photoacoustic measurement data by recognizing the type of frequency response curve: if a flat curve is detected, the photoacoustic signal is not distorted and is automatically forwarded to the output, if the signal is distorted, the classification model has the task to recognize which type of microphone has such a response. Depending on the recognized microphone type particular database is selected, which will be used for regression model training, Figure 6b). Database for each observed type of microphone is obtained on the way explained in the article. The creation and hyperparameters tuning of classification model was subject of our earlier research [30]. It is simple neural network architecture due to learning with large dataset, which embeds into the model huge knowledge about PA experimental conditions. Classifier is thus optimized to one hidden layer with 2 neurons. Its hyperparameters are presented in Table 2. Also, learning process was extremely efficient, it lasted 100 epochs or a few minutes. The input vector of classification model consists of 400 elements, 200 of them present samples of amplitude and the remaining 200 are samples of phase characteristics of the analyzed photoacoustics response. Performance of the classification model is defined in Table 3.

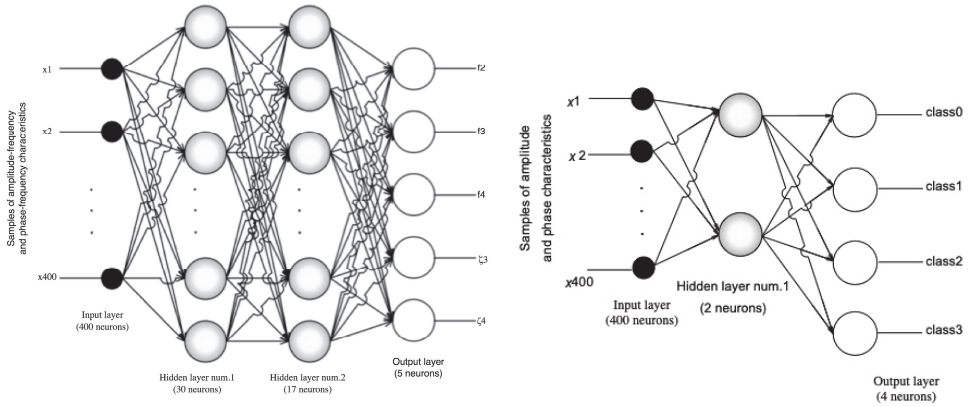

Figure 6: Classification and regression model [30] [31]

Table 2: Neural networks structure and tuning [28]

Model	No. of inputs	No. of out-puts	No. of hidden layers	No. of neurons in hidden layers	Activation function	Training set dimension	Dev. set dimension = Test set dimension	Learning rate	Momentum parameters	Mini - batch size	No. of epochs
Regression	400	5	2	n[1] =30, n[2] = 17	tanh()	57,500	5,000	10^{-4}	$\beta_1 = 0.9$ $\beta_2 = 0.999$ $\varepsilon = 10^{-8}$	32	3000
Classification	400	4	1	n[1] =2,	tanh(), softmax()	243,000	13,500	10^{-4}	$\beta_1 = 0.9$ $\beta_2 = 0.999$ $\varepsilon = 10^{-8}$	128	100

Table 3: Performance of the classification model [30]

Frequency range	Accuracy (train, dev, test)	Number of epochs	Prediction time
20 – 20000 Hz	99.99%, 99.99%. 99.99%	100	17ms

In our previous research [31] regression model and detailed analysis of hyperparameters choice are illustrated. Model was tested on samples of different materials and diverse microphones, so its accuracy and reliability has been proven, Table 4. Its design is depicted on Figure 6a) and its hyperparameters are shown in Table 2. The input vector has the same number of features as input vector of the classifier.

Both, classification and regression model are precise enough and work in real time, so thus satisfy requirements of the PA experiment. They are reliable, classification model 100% recognizes microphone type maintained with simulated data, [30] and the average error that regression model makes on these tests is negligible [31].

Table 4: Performance of the regression model [31]

Average deviation from the accurate value expressed in percentage of the accurate value on the training set for microphone EMC30B (frequency ranqe 20-20000 Hz), accuracy = 98.68%					
Parameter	f2	f3	f4	ζ3	ζ4
	0.07132456	0.14649154	0.05109024	0.74361974	0.967724
Average deviation from the accurate value expressed in percentage of the accurate value on the validation set for microphone EMC306 (frequency range 20-20000 Hz), accuracy = 98.73%					
Parameter	f2	f3	f4	ζ3	ζ4
	0.07109252	0.14936025	0.05018261	0.73954904	0.95961267
Average deviation from the accurate value expressed in percentage of the accurate value on the test set for microphone EMC306 (frequency range 20-20000 Hz), accuracy = 98.46%					
Parameter	f2	f3	f4	ζ3	ζ4
	0.07197632	0.14702412	0.05081375	0.78105694	1.0586549
Prediction time microphone EMC306 (frequency range 20-20000 Hz)					
CPU time			Computation time		
14 ms			40 ms		
Average deviation from the accurate value expressed in percentage of the accurate value on the training set for microphone EMC60 (frequency ranqe 20-20000 Hz), accuracy = 98.5%					
Parameter	f2	f3	f4	ζ3	ζ4
	0.08030392	0.06785115	0.06096664	0.7990959	1.0014774
Average deviation from the accurate value expressed in percentage of the accurate value on the validation set for microphone EMC60 (frequency range 20-20000 Hz), accuracy = 98.5%					
Parameter	f2	f3	f4	ζ3	ζ4
	0.07929239	0.0674798	0.06169094	0.76554894	1.0300709
Average deviation from the accurate value expressed in percentage of the accurate value on the test set for microphone EMC60 (frequency range 20-20000 Hz), accuracy = 98.44%					
Parameter	f2	f3	f4	ζ3	ζ4
	0.08065586	0.06766558	0.06113705	0 8405477	1.0059946
Prediction time microphone EMC60 (frequency range 20-20000 Hz)					
CPU time			Computation time		
13 ms			35 ms		
Average deviation from the accurate value expressed in percentage of the accurate value on the training set for microphone WM66 (frequency ranqe 20-20000 Hz), accuracy = 98.87%					
Parameter	f2	f3	f4	ζ3	ζ4
	0.07622549	0.07398161	0.06836206	0.6666061	0.7081819
Average deviation from the accurate value expressed in percentage of the accurate value on the validation set for microphone WM66 (frequency range 20-20000 Hz), accuracy = 98.93%					
Parameter	f2	f3	f4	ζ3	ζ4
	0.07429651	0.07452826	0.06824242	0.6592338	0.6810206
Average deviation from the accurate value expressed in percentage of the accurate value on the test set for microphone WM66 (frequency range 20-20000 Hz), accuracy = 98.68%					
Parameter	f2	f3	f4	ζ3	ζ4
	0.07601995	0.07425365	0.06885304	0.7398573	0.7364045
Prediction time microphone WM66 (frequency range 20-20000 Hz)					
CPU time			Computation time		
14 ms			41 ms		

4.2. Application in the development of a self consistent inverse procedure (SCIP)

In the publication [29], a regression based method for parameter estimation is presented, which is aimed, in particular, at the determination of linear thermal expansion coefficient and thermal diffusivity, based on transmission photoacoustic measurements performed on solids. The idea makes use of a novel methodology in the solving of inverse problems: firstly, the ANN-based study is performed regarding the presence of the microphone characteristics in the recorded signal, which is, secondly, removed. Afterwards, the SCIP is performed on the obtained data, widening the frequency range in use in comparison to previously developed methods, and improving the accuracy. The efficiency of the developed method is proven on aluminum.

The behavior of thermo-physical properties, such as DT, and aT, in the frequency range of the performed PA measurements (20 Hz – 20 kHz), is quite complex when surface absorbents, like metals, are used. The estimation of these parameters by means of regression based fitting is error-prone, which is amplified in real-life experimental conditions, where the influence of measurement chain is notable. This influence is significantly reduced by means of the developed ANN-based method, which estimates a set of parameters needed for the filtration of the mentioned disturbance.

In Figure 7, the PA response lines (both amplitude and phase) based on theory are shown in parallel to the experimentally obtained signal and the ANN-processed data. At low and at high frequencies, signal disturbances can be observed (red lines), attributed mostly to the microphone [32], which are successfully suppressed using the mentioned method: the green lines show significant similarity to the blue lines, as opposed to the red ones.

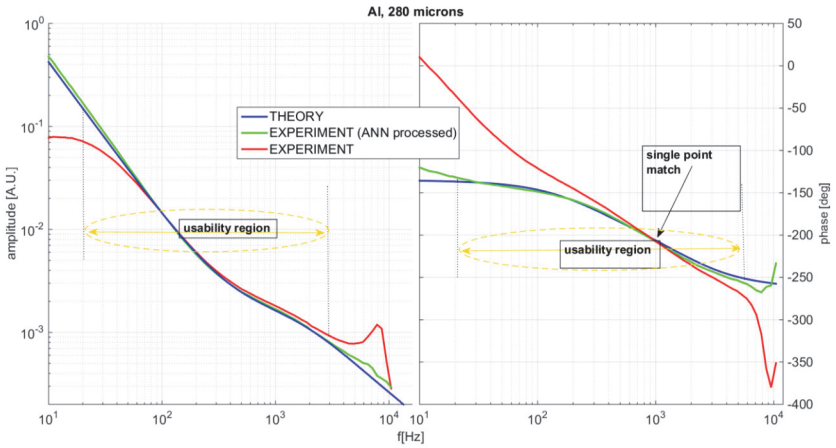

Figure 7: Theoretically obtained PA response of aluminum at 280 μm (blue line) vs. experimentally gained data (red line) vs. ANN-corrected experimental data (green line), [32]

Overall, the amplitude line is successfully processed under 2500 Hz in comparison to higher frequencies, while in the case of the phase line, the correction may be considered satisfying above 100 Hz. Therefore, the usability region is much wider than it used to be at the first place: it is visible that, in this region, the mean square deviation of both PA response lines from the obtained ANN-processed data is much smaller in comparison to the case when it is subtracted from experimentally obtained signal directly.

The validation of the procedure is firstly done on a controlled numerical experiment [29, 32] with the relative estimation error between estimated and preset values acting as the index of success:

Table 5: SCIP results on numerical experiment [32]

Parameter combination		D_{TS} - assembly, a_T - assembly	D_{TS} - assembly, a_T - random	D_{TS} - random, a_T - assembly	D_{TS} - random, a_T - random
reL estimate error [%]	D_{TS}	0	0	0.01	0.009
	a_T	0	0.006	0.01	0.011
max. iter. N⁰		4	3	3	4

When the SCIP is performed on the experimentally obtained signals (frequency PA response measurement on Aluminum at 197 μm and 280 μm) the results are considered very good. As shown in Table 6, the estimated parameters are quite close at both thickness levels, while the resulting reconstruction, presented in Figure 8, shows remarkable resemblance between lines based on preset and estimated parameter values.

Table 6: SCIP results on experiment [32]

Sample thickness [μm]		197	280
Parameter estimate	D_{TS} [x10^{-5} m^2/s]	8.59	8.36
	a_T[x10^{-6}K^{-1}]	23.4	21
iter.N°		4	2

The self-consistency of the SCIP is demonstrated through its convergence in the application on the established numerical experiment, with relative error not exceeding 0.02 % and finishing always under six iterations. Afterwards it is confirmed in the application on experimentally obtained PA response of Aluminum samples at two thickness levels (197 and 280 μm), with resultin estimates in accordance with literature expectations and iterations remaining equally low.

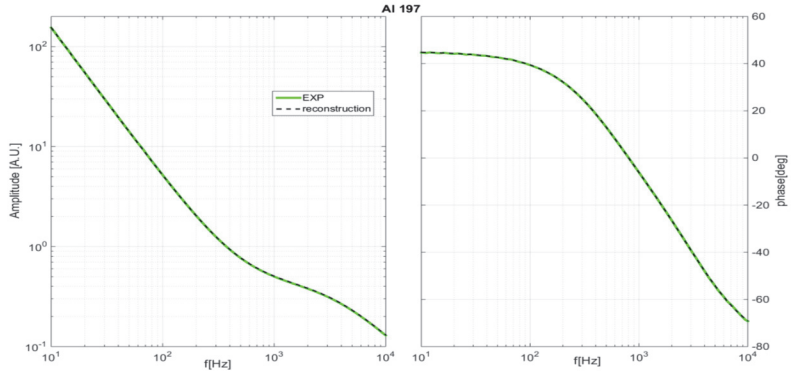

(a)

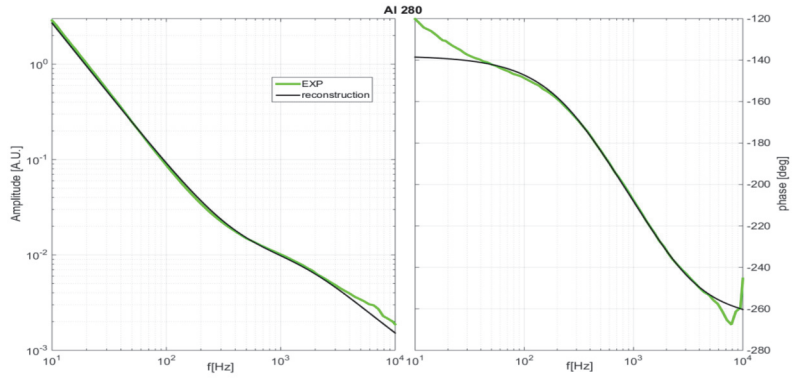

(b)

Figure 8: ANN preprocessed experimental results (green) obtained from a 197 μm (a) and 280 μm (b) thick sample alongside reconstructed data, based on the estimated parameters (black) [32]

4.3. Application of the neural network in the inverse solution of the photoacoustic problem

After applying the network in microphone classification, Table 3, and recognizing the instrumental influence, Table 4, on the measured photoacoustic signal, deconvolution of useful signal and removing of instrumental influence can be done by (4-9). The obtained signal of the aluminum sample can be analyzed by standard fitting methods by comparison with the theoretical model (1-3), developed procedures (SCIP), or by applying neural networks in determining the sample parameters. Thus, the sample can be characterized very precisely by determining the parameters from the amplitude and phases of the photoacoustic signals in the frequency domain. The neural network was applied in the frequency domain 10 to 20kHz and trained on 1089 photoacoustic signals of the theoretical model, unit (1-3) for the aluminum sample, with the aim of predicting three parameters: thermal diffusivity, thermal expansion coefficient and sample thickness, Figure 9. Sample thickness parameter is introduced as a control parameter. During training, testing and validation, the neural network learns from the data stored in the neurons. Neurons represent values that are associated with a non-linear function. Training takes place during several epochs until one of the criteria is met, which determines the termination of further training [33].

The simple structure of the neural network in supervised training forms a tool obtained by error minimization, so that the parameters: thickness l^{NN}, thermal diffusivity D_T^{NN}, and linear expansion α_T^{NN} of the experimentally measured aluminum sample with a thickness of 197 μm, Figure 8(a) can be determined precisely with errors <1%, Table 7 [33,34].

Table 7. Thickness l^{NN}, thermal diffusivity D_T^{NN}, and linear expansion α_T^{NN} parameters determined by neural network analyzed by standard fitting methods by comparison with the theoretical model, and measured photoacoustic signal, with deconvolution of the useful signal with removed instrumental influence.

type exp PAS	$l^{NN}[\mu m]$	$D_T^{NN}\left[10^{-5}m^2s^{-1}\right]$	$\alpha_T^{NN}\left[K^{-1}\right]$
standard PAS	196.78	8.5559	2.3149
measured useful signal	197.45	8.5812	2.3114

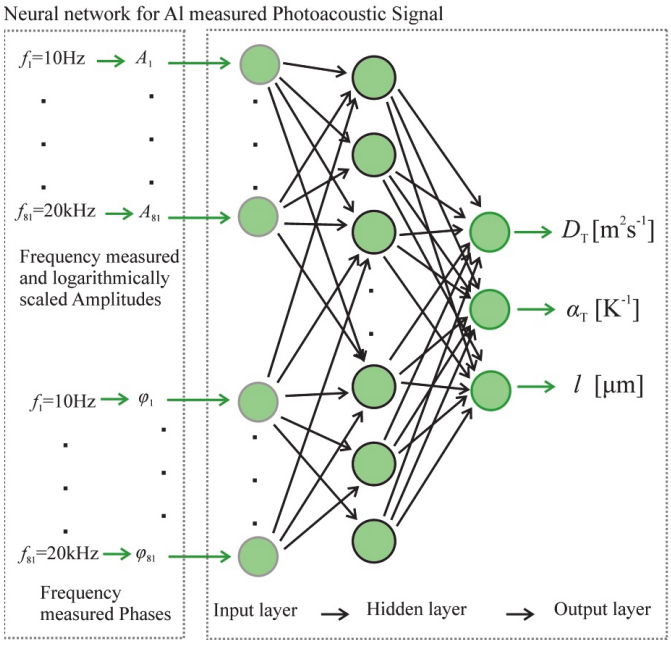

Figure 9. Training network for determining aluminum parameters

5. CONCLUSION

The idea of using simulated data in the processing real PA measurement data is completely explained and justified. Developed theoretical-mathematical model was a base for software design, intended for data generation. Expert knowledge is crucial for credibility to the experiment. Several machine learning models were trained on the obtained database. Models are precise regarding requirements of the PA experiment and work in real time. In terms of reliability, the average model errors are negligible in testing maintained with real and numerical experiments. The potential of using simulated data is of great importance for processing PA measurement data: simplifying and accelerating two procedures - the procedure of extraction of microphone transfer function from distorted PA signal for the reason of its correction from instrumental deviations and procedure of material characteristics determination.

REFERENCES

[1] Y. S. Abu-Mostafa, M. Magdon-Ismail, and H.-T. Lin, "Learning From Data", AML Book, (2012)

[2] D. Allman, A. Reiter and M.A.L. Bell, "Photoacoustic Source Detection and Reflection Artifact Removal Enabled by Deep Learning," IEEE Trans. Med. Imaging, Vol. 37, pp. 1464–1477, https://doi.org/10.1109/TMI.2018.2829662, (2018)

[3] M. Lukić, Ž. Ćojbašić, M.D. Rabasović, D.D. Markushev and D.M. Todorović, "Laser Fluence Recognition Using Computationally Intelligent Pulsed Photoacoustics Within the Trace Gases Analysis," Int J Thermophys, Vol. 38, p. 165, https://doi.org/10.1007/s10765-017-2296-5, (2017)

[4] M. Lukić, Ž. Ćojbašić, M.D. Rabasović and D.D. Markushev, "Computationally intelligent pulsed photoacoustics," Meas. Sci. Technol, Vol. 25, p.125203. https://doi.org/10.1088/0957-0233/25/12/125203, (2014)

[5] M. N. Popovic, D. Furundzic, and S. P. Galovic, "Photothermal Depth Profiling Of Optical Gradient Materials By Neural Network," Publ. Astron. Obs. Belgrade, vol. 89, no. May 2015, 2010

[6] Y. LeCun, Y. Bengio and G. Hinton, "Deep learning," Nature, Vol. 521, pp. 436–444, https://doi.org/10.1038/nature14539, (2015)

[7] S. Aleksic, D. Markushev, D. Pantic, M. Rabasovic, D. Markushev and D. Todorovic," Electro-acustic influence of the measuring system on the photoacoustic signal amplitude and phase in frequency domain," Facta Univ Phys Chem Technol, Vol. 14, pp. 9–20. https://doi.org/10.2298/FUPCT1601009A, (2016)

[8] A. Handa, V. Patraucean, V. Badrinarayanan, S. Stent and R. Cipolla, "Understanding RealWorld Indoor Scenes with Synthetic Data," 2016 IEEE Conference on Computer Vision and Pattern Recognition (CVPR), IEEE, Las Vegas (United States of America), pp. 4077–4085, https://doi.org/10.1109/CVPR.2016.442, (2016)

[9] A. Shrivastava, T. Pfister, O. Tuzel, J. Susskind, W. Wang and R. Webb, "Learning from Simulated and Unsupervised Images through Adversarial Training," 2017 IEEE Conference on Computer Vision and Pattern Recognition (CVPR), IEEE, Honolulu (United States of America), pp. 2242–2251, https://doi.org/10.1109/CVPR.2017.241, (2017)

[10] G. Cosne et al., "Using Simulated Data to Generate Images of Climate Change," in ML-IRL workshop at ICLR, pp. 1–9, (2020)

[11] A. Rosencwaig, "Photoacoustic spectroscopy of solids," Optics Communications, Vol. 7, pp. 305–308, https://doi.org/10.1016/0030-4018(73)90039-4, (1973)

[12] L.F. Perondi and L.C.M. Miranda, "Minimal-volume photoacoustic cell measurement of thermal diffusivity: Effect of the thermoelastic sample bending", Journal of Applied Physics, Vol. 62, pp. 2955–2959, https://doi.org/10.1063/1.339380, (1987)

[13] M.N. Popovic, M.V. Nesic, S. Ciric-Kostic, M. Zivanov, D.D. Markushev, M.D. Rabasovic and S.P. Galovic, "Helmholtz Resonances in Photoacoustic Experiment with Laser-Sintered Polyamide Including Thermal Memory of Samples," Int J Thermophys, Vol. 37, p. 116, https://doi.org/10.1007/s10765-016-2124-3, (2016)

[14] A. Rosencwaig and A. Gersho, "Photoacoustic Effect with Solids: A Theoretical Treatment," Science, Vol. 190, pp. 556–557, https://doi.org/10.1126/science.190.4214.556, (1975)

[15] F.A. McDonald and G.C. Wetsel, "Generalized theory of the photoacoustic effect," J. Appl. Phys, Vol. 49, p. 2313, https://doi.org/10.1063/1.325116, (1978)

[16] G. Rousset, F. Lepoutre and L. Bertrand, "Influence of thermoelastic bending on photoacoustic experiments related to measurements of thermal diffusivity of metals," Journal of Applied Physics, Vol. 54, pp. 2383–2391. https://doi.org/10.1063/1.332352, (1983)

[17] P. M. Nikolic and D. M. Todorović, "An investigation of semiconducting materials using a photoacoustic method. u: Technical sciences book 40, Monographs, Belgrade: Serbian Academy of Sciences and Arts Department, vol. DCXLVIII." Serbian Academy of Sciences and Arts, 2001.

[18] D.D. Markushev, M.D. Rabasović, M. Nesic, M. Popovic and S. Galovic, "Influence of Thermal Memory on Thermal Piston Model of Photoacoustic Response," Int J Thermophys, Vol. 33, pp. 2210–2216. https://doi.org/10.1007/s10765-012-1229-6, (2012)

[19] M. Nesic, S. Galovic, Z. Soskic, M. Popovic and D.M. Todorovic, "Photothermal Thermoelastic Bending for Media with Thermal Memory," Int J Thermophys, Vol. 33 pp. 2203–2209, https://doi.org/10.1007/s10765-012-1237-6, (2012)

[20] S. Galović, Z. Šoškić, M. Popović, D. Čevizović and Z. Stojanović, "Theory of photoacoustic effect in media with thermal memory," Journal of Applied Physics, Vol. 116, p. 024901, https://doi.org/10.1063/1.4885458, (2014)

[21] D.M. Todorović, M.D. Rabasović and D.D. Markushev, "Photoacoustic elastic bending in thin film—Substrate system," Journal of Applied Physics, Vol. 114, p. 213510, https://doi.org/10.1063/1.4839835, (2013)

[22] D.M. Todorović, M.D. Rabasović, D.D. Markushev and M. Sarajlić, "Photoacoustic elastic bending in thin film–substrate system: Experimental determination of the thin film parameters," Journal of Applied Physics, Vol. 116, p. 053506, https://doi.org/10.1063/1.4890346, (2014)

[23] M. Popovic, "Generalizovani fotoakustični odziv dvoslojnih struktura", Zadužbina Andrejević, Belgrade (Serbia), (2018)

[24] M. N. Popovic, "Fotoakustički odziv transmisione fotoakustičke konfiguracije i analiza rezonantnih fenomena za dvoslojne uzorke sa toplotnom memorijom," Univerzitet u Novom Sadu, Serbia, (2016)

[25] M. N. Popovic, D. D. Markushev, M. V. Nesic, M. I. Jordovic-Pavlovic, and S. P. Galovic, "Optically induced temperature variations in a two-layer volume absorber including thermal memory effects," J. Appl. Phys., Vol. 129, no. 1, (2021)

[26] M.N. Popovic, M.V. Nesic, M. Zivanov, D.D. Markushev and S.P. Galovic, "Photoacoustic response of a transmission photoacoustic configuration for two-layer samples with thermal memory," Opt Quant Electron, Vol. 50, p. 330, https://doi.org/10.1007/s11082-018-1586-x, (2018)

[27] M. D. Rabasovic, M. G. Nikolic, M. D. Dramicanin, M. Franko and D. D. Markushev, "Low-cost, portable photoacoustic setup for solid samples," Meas. Sci. Technol., Vol. 20(9), p. 95902, (2009)

[28] M.I. Jordovic-Pavlovic, A.D. Kupusinac, K.Lj. Djordjevic, S.P. Galovic, D.D. Markushev, M.V. Nesic and M.N. Popovic, "Computationally intelligent description of a photoacoustic detector," Opt Quant Electron, Vol. 52, p. 246, https://doi.org/10.1007/s11082-020-02372-y, (2020)

[29] M. Nesic, M. Popovic, K. Djordjevic, V. Miletic, M. Jordovic-Pavlovic, D. Markushev and S. Galovic, "Development and comparison of the techniques for solving the inverse problem in photoacoustic characterization of semiconductors," Opt Quant Electron, Vol. 53, p. 381, https://doi.org/10.1007/s11082-021-02958-0, (2021)

[30] M. Jordović-Pavlović, A. Kupusinac, S. Galović, D. Markushev, M. Nešić, K. Djordjević and M. Popović, "Potential of Using Simulated Data in Processing Photoacoustic Measurement Data", Proceedings of 8th International-Conference on Electrical, Electronic, and Computing Engineering (IcETRAN), (2021)

[31] M.I. Jordović-Pavlović, M.M. Stanković, M.N. Popović, Ž.M. Ćojbašić, S.P. Galović and D.D. Markushev, "The application of artificial neural networks in solid-state photoacoustics for the recognition of microphone response effects in the frequency domain," J Comput Electron, Vol. 19, pp. 1268–1280, https://doi.org/10.1007/s10825-020-01507-4, (2020)

[32] M.V. Nesic, M.N. Popovic, S.P. Galovic, K.Lj. Djordjevic, M.I. Jordovic-Pavlovic, V.V. Miletic and D.D. Markushev, "Estimation of linear expansion coefficient and thermal diffusivity by photoacoustic numerical self-consistent procedure," Journal of Applied Physics, Vol. 131, p. 105104, https://doi.org/10.1063/5.0075979, (2022)

[33] K.Lj. Djordjević, S.P. Galović, M.N. Popović, M.V. Nešić, I.P. Stanimirović, Z.I. Stanimirović and D.D. Markushev, "Use neural network in photoacoustic measurement of thermoelastic properties of aluminum foil," Measurement, Vol. 199, p. 111537, https://doi.org/10.1016/j.measurement.2022.111537, (2022)

[34] K.L. Djordjevic, S.P. Galovic, M.I. Jordovic-Pavlovic, Z.M. Cojbasic and D.D. Markushev, "Improvement of Neural Networks Applied to Photoacoustic Signals of Semiconductors with Added Noise," Silicon, Vol. 13, pp. 2959–2969, https://doi.org/10.1007/s12633-020-00606-y, (2021)

[35] V. Milicević, S. Milovanović and B. Milosavljević, "Improving business helpdesk systems with intelligent search mechanisms," Ekonomski Pogledi Vol. 17, pp. 123–137, https://doi.org/10.5937/EkoPog1502123M, (2015)

[36] V. Milićević, N. Zdravković, J. Jović and D. Jagličić, "Modeling a software platform for beehive placement optimization," Acta Agriculturae Serbica, Vol. 27, pp. 39–48, https://doi.org/10.5937/AASer2253039M, (2022)

[37] N. Petrović, V. Jovanović, M. Petrović, B. Nikolić and J. Pavlović, "Evaluating the operation performance of the Serbian transport Freight system by using multiple criteria decision-making technique," Engineering Today, Vol. 1, pp. 33–40, https://doi.org/10.5937/engtoday2204033P, (2022)

[38] G. Pavlović, B. Jerman, M. Savković, N. Zdravković and G. Marković, "Metaheuristic applications in mechanical and structural design," Engineering Today, Vol. 1, pp. 19–26, https://doi.org/10.5937/engtoday2201019P, (2022)